CONTROLLING THE POLYMORPHISM OF ACTIVE PHARMACEUTICAL INGREDIENTS WITH TWO-DIMENSIONAL TEMPLATES

M.S. THESIS

SUBMITTED BY

JASON R. COX

DEPARTMENT OF CHEMISTRY AND BIOCHEMISTRY
WORCESTER POLYTECHNIC INSTITUTE

TABLE OF CONTENTS

1 INTRODUCTION

1.1 Objectives

The aim of this work is to examine the effect of interfaces on the crystallization of compounds that exhibit polymorphism. Specifically, we are interested in monolayers derived from thiol-based surfactants bearing functional groups that may promote face selective growth through epitaxy. The ultimate objective of this work is to get a better understanding of interfacial interactions and molecular recognition during crystal growth in order to pave the way toward the development of new tools to control the outcome of crystal growth.

1.2 Definitions

The term polymorphism, in relation to solid state chemistry, was first coined by Mitscherlich in 1822.[1] He recognized that inorganic compounds could adopt more than one arrangement of ions in the solid state. In 1965, a more encompassing definition was developed by McCrone.[2] He defined polymorphism as, 'a solid crystalline phase of a given compound resulting from the possibility of at least two different arrangements of that compound in the solid state'. This definition also includes conformational polymorphism which is the ability of a molecule to adopt different conformations in different solid forms. In addition, pure compounds can form hydrates or solvates wherein water or solvent molecules are present periodically (and usually in a stoichiometric ratio) throughout the crystal lattice. We refer to these multicomponent solids as hydrates and solvates.[3]

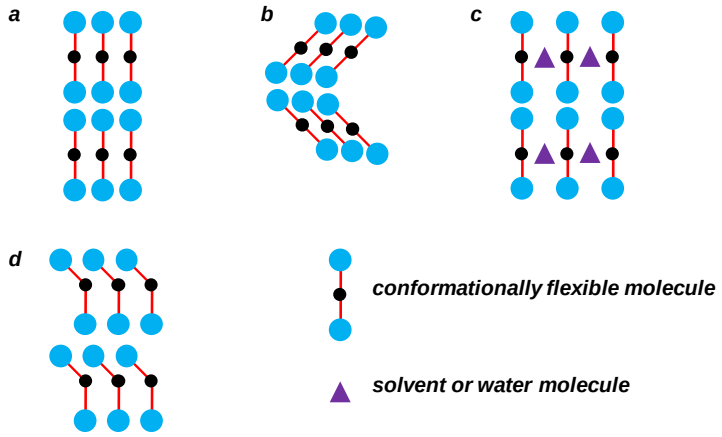

Figure 1. Schematic depiction of different types of polymorphism. (a-b) polymorphs, (c) hydrate or solvate, and (d) conformational polymorph of (a).

1.3 Polymorphism and Structure-Property Relations

One encounters the structure-property relationships of different polymorphs on a daily basis. A familiar example is given by the two allotropes of carbon – graphite and diamond. Both materials are exclusively made of carbon yet they exhibit distinct physical properties. Diamond is the hardest material known on earth and is coveted for its clarity and beauty as a gemstone, whereas graphite is typically used in pencils and as a lubricant.

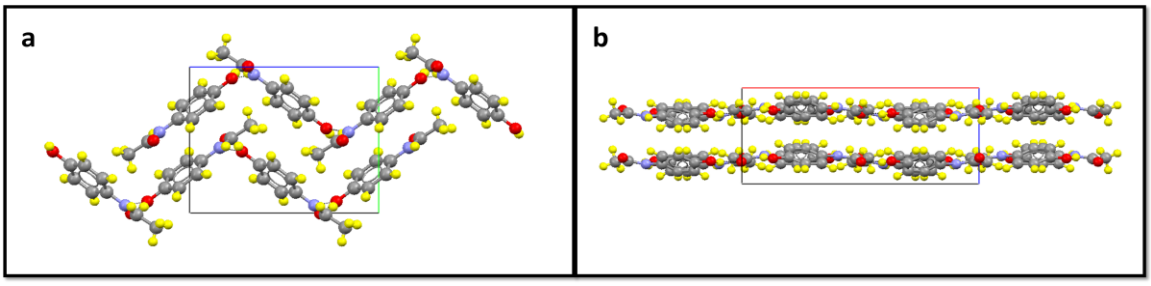

Figure 2. Crystal structures of two polymorphs of acetaminophen. (Gray = C, Red = O, Blue = N, Yellow = H) (a) Crystal structure of acetaminophen form I. View along *a*-axis. (b) Crystal structure of acetaminophen form II. View along *b*-axis. Note the slip plane between the molecular sheets in form II.[4]

In the case of molecular crystals, the spatial organization of the molecules is determined by noncovalent interactions such as hydrogen bonds. These interactions act as intermolecular glue, and due to their directionality and strength, determine the orientation of molecules in the solid state. In the case of polymorphs, noncovalent bonding motifs are different and generate unique packing arrangements (**Figure 2**). The results of unique packing arrangements are manifested in the physical properties and characteristics of the different modifications. Polymorphs exhibit differences in density, melting point, thermal conductivity, enthalpy, and solubility to name a few.[5] The pharmaceutical industry is particularly concerned with polymorphism because polymorphs of active pharmaceutical ingredients (APIs) exhibit differences in bioavailability, shelf-life and communition.[6] These differences may make one polymorph more suitable than another as a drug candidate, they also emphasize the importance of polymorph screening in drug development.

1.4 Impact of Polymorphism on Drug Development and Marketing

In recent years, the topic of polymorphism has been involved in a number of high profile cases. Showcasing this situation is ritonavair; a protease inhibitor drug manufactured by Abbott Laboratories under the trade name Norvir®. After approximately 18 months on the market, a new polymorph of the drug had begun to dominate the production line. This new modification is more stable than the original marketed form and exhibits decreased dissolution rates as well as inferior bioavailability. Abbott was forced to recall the drug from the market and subsequently developed a liquid suspension of the drug after an intense year long research effort.[7] This event is symbolic of the importance of determining the most stable form of a drug early in drug development processes.

Polymorphism has also become a topic of concern in patent litigation. As stated earlier, polymorphs of the same pure substance each possess discrete packing motifs in the solid state. In patent law, a polymorph may be considered worthy of patent protection if the new form is 'unobvious'. A patent litigation involving Glaxo Smithkline typifies the situation. Ranitidine hydrochloride, the active ingredient in the popular heartburn medication Zantac®, was the center of debate in the late 1980's and early 1990's. Glaxo Smithkline (GSK) already possessed the production rights to the drug when they serendipitously discovered a second form of the compound, which they patented for its improved drying and filtration characteristics. Novapharm Ltd, a generic pharmaceutical company, sought to prepare the old form by following the procedures outlined in the original patent but obtained only the new form. Novapharm argued that the ranitidine hydrochloride present in Zantac® is, and also has been, the new form and that the original patent was incorrect. A lengthy legal battle ensued, and at the end GSK won the case and protected their patents.[8]

The above scenarios emphasize the need to screen for polymorphs early in drug development. In Abbott's case, early detection of the more stable form may have prevented the fallout resulting from the late stage phase transformation. The situation involving GSK and Novapharm Ltd illustrates how subtle differences in drug preparation can have a profound impact on the polymorph obtained.

1.5 Previous Approaches to Controlling Polymorphism

Selective growth of polymorphs, for the most part, has been a trial and error process. Typically, screens are carried out by varying physical conditions such as temperature, pressure, solvents, and initial saturation levels. Recently, this approach has been adapted for use in a high-throughput environment.[9] This trial and error approach is limited in that it is empirical and does not control or influence nucleation in a planned manner.

Nucleation, broadly defined, is the aggregation of solute molecules into small clusters with packing motifs that closely resemble the spatial organization of molecules in the resulting crystal.[10] Altering nucleation through the use of templates is believed to influence the crystal form obtained during crystallization. Tailor-made additives have been used to increase or decrease the likelihood of nucleating a specific form.[11] More importantly, two-dimensional templates bearing functional groups complementary to the exposed functionality of a particular crystal face of growing nuclei have been shown to alter the outcome of crystal growth.[12] The interaction between the designer surface and the crystal face serves to stabilize the interacting nucleus, a process known as epitaxy.[13] By stabilizing the nuclei of one polymorph, and not the others, one can increase the likelihood of controlling polymorphism.

Typically, self-assembled monolayers (SAMs) are used as templates in these experiments. SAMs can be fabricated on coinage metals, hydroxylated substrates, and at air-solution interfaces.[14] Depending on the type of monolayer system used, the molecules may be arranged differently or not at all. For example, thiol molecules chemisorbed on Au surfaces exhibit domains of two-dimensional periodicity similar to the order found in

crystals. Silane monolayers fabricated on hydroxylated surfaces, however, do not exhibit any long range order. These differences and similarities increase the number of conditions that can be used in experiments. Accordingly, researchers have used SAMs of thiols/Au, silanes/OH, and single crystal substrates (including crystals of other polymorphs) to selectively nucleate a desired polymorph. Other approaches include the use of polymeric heteronuclei,[15] laser induced nucleation,[16] ultra-high pressure crystallization,[17] and nanoscale confinement.[18]

1.6 Rationale for Current Work

Ideally, prior knowledge of the orientation and hydrogen bonding motifs of a polymorph is necessary to design an appropriate nucleation template; however, this is not the case when screening for new polymorphs. In our experiments, we chose to screen for polymorphs of APIs using SAMs on Au and glass substrates bearing different terminal functional groups. We performed recrystallizations of APIs in the presence of these templates with the hope of selectively nucleating a particular form. Our APIs were chosen based on a few simple stipulations. We wanted drug compounds that are polymorphic, easily characterized, and in some cases exhibit a propensity to form hydrates and solvates. We also wanted a diverse set of templates that would allow us to test a number of variables related to the composition of the substrate. Of particular interest were substrates that exhibit long-range order, hydrophilicity or hydrophobicity, and complementary functionalities.

2 SELECTIVE NUCLEATION - THEOPHYLLINE

2.1 Background

Theophylline, a purine derivative isolated from tea leaves, is a widely used bronchodilator.[19] The compound is known to exist in four possible modifications.[20] Of these four modifications, two forms occur frequently under standard pressure and temperature: (i) an anhydrous modification – Form II; orthorhombic ($Pna2_1$) and (ii) a monohydrate; monoclinic ($P2_1/n$). These two forms are known to crystallize concomitantly from ethanol at 70% relative humidity.[21] The other two forms are extremely rare and are only encountered at very high temperatures, conditions which are not explored in this work.

In this work we sought to investigate the effect of hydrophilic and hydrophobic substrates on the crystal growth of theophylline. We surmised that hydrophilic functionalities may interact with specific faces of particular polymorphs of theophylline. The hydrophobic interfaces were not expected to play a role except as controls.

We initiated our work by recrystallizing theophylline from saturated ethanolic solutions in the presence of hydrophobic and hydrophilic surfaces. Surfaces were comprised of alkanethiol molecules self assembled on Au substrates. Ideally, we wanted to selectively nucleate one of the metastable forms of theophylline on a hydrophilic monolayer. Surprisingly, we reproducibly obtained the stable anhydrous form on hydrophilic substrates and the monohydrate on hydrophobic substrates. This unexpected result is due to favorable interactions between crystal faces of the anhydrous orthorhombic form and functional groups belonging to the monolayer. The results are also discussed in the context of a disparity in the number of hydrogen-bond donors and acceptors in the packing motif of orthorhombic theophylline.

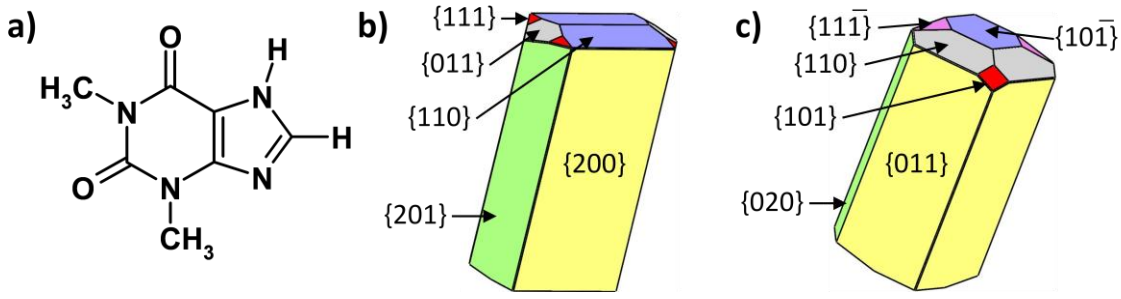

Figure 3. (a) Molecular structure of theophylline and morphologies of the (b) anhydrous form and (c) monohydrate calculated using BFDH theory. Symmetry independent faces are labeled.

2.2 Results

Hydrophobic substrates were derived from 1-dodecanethiol (**1**) and 1-hexadecanethiol (**2**), hydrophilic substrates were made from 11-mercaptoundecanol (**3**), 11-mercaptoundecanoic acid (**4**), and 16-mercaptoundecanoic acid (**5**). Crystallizations were performed at 20° C and ambient humidity (summers in Worcester can be quite humid) in 20mL scintillation vials using a slow evaporation procedure (an aluminum foil with small holes regulates the rate of evaporation). All experiments were repeated five times to ensure reproducibility of results.

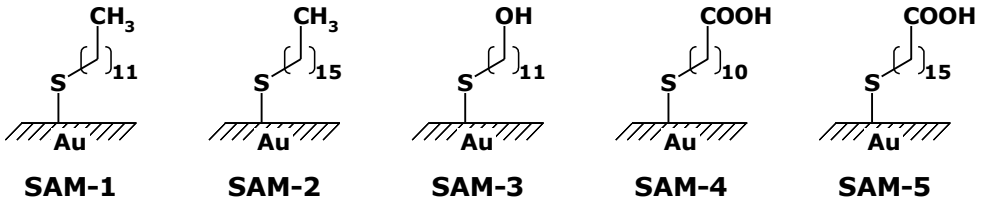

Figure 4. Schematic structures of SAMs used as templates in this work.

We observed that hydrophilic SAMs **3-5**, surfaces bearing hydrogen bond donors and acceptors, selectively nucleated the anhydrous modification of theophylline. The walls of the vials contained the monohydrate indicating that both forms nucleated under the conditions used in this study. The exclusive growth of the anhydrous form on the SAM surface reveals a potential complementary interaction at the interface of the monolayer and the growing anhydrous crystal.

Vials containing hydrophobic substrates **1** and **2** exhibited exclusive growth of the monohydrate. In these experiments, monohydrate crystals were also present on the vial walls, consistent with our previous observations of crystal growth in the presence of SAMs **3-5**. Theophylline, when recrystallized in the absence of a template, resulted in concomitant growth of both modifications with the monohydrate being the predominant form. Crystal growth using bare Au as a template yielded similar results in accordance with the hydrophobic character of bare Au. Optical micrographs illustrate the effect of designer interfaces on the crystal growth of theophylline (**Figure 5)**.

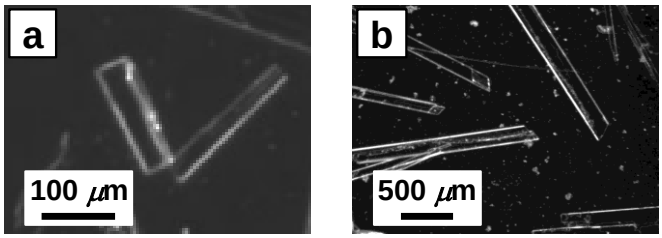

Figure 5. Optical micrographs showing (a) the selective growth of the anhydrous form of theophylline on carboxy-terminated SAM-**4**, and (b) the growth of the monohydrate on methyl-terminated SAM-**2**.

The results obtained in this study can be rationalized in terms of a disparity in the number of hydrogen bond donors and acceptors in the anhydrous form. Theophylline has two acidic hydrogen bond donors (the imidazole NH and =CH groups) and three acceptors (the two coordinate imidazole nitrogen atom and the two carbonyl oxygen atoms). If we consider that each carbonyl atom can act as a *bis*-hydrogen bond acceptor, there is a shortage in the number of hydrogen bond donors. The hydrogen bond acceptors that are not involved in a hydrogen bond become likely candidates for template growth.

Figure 6 shows the molecular arrangement at various planes corresponding to the macroscopic growth faces of the anhydrous form. These images show a corrugated packing at (110), (111), and (011) planes; thus, a greater degree of surface reconstruction is necessary before the corresponding crystal faces can interact with the SAM surfaces. Three other factors, (i) parallel alignment of molecules with respect to the planes, (ii) lack of distinctly exposed hydrogen bond acceptors at the interface, and (iii) relatively smaller size of the corresponding macroscopic faces (**Figure 3**), make these faces less likely to be nucleated by the hydrogen bonding SAMs **3**-**5**.

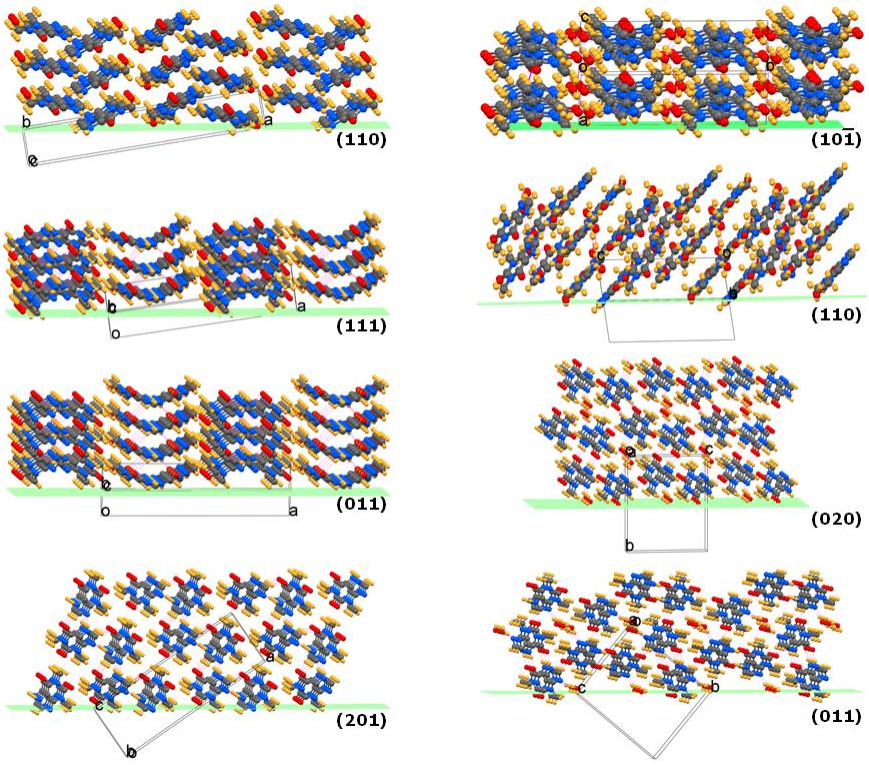

Figure 6. Molecular arrangement at various planes in the crystal structure of the anhydrous (left) and monohydrate forms (right) of theophylline.

In contrast, the {200} and {201} faces are large (**Figure 3**) and the molecules lie nearly perpendicular to the corresponding crystal planes (**Figures 6** and **7**). Both sets of faces

expose the third hydrogen bond acceptor at the interface and hence both faces can potentially be nucleated by the SAMs **3**-**5**.

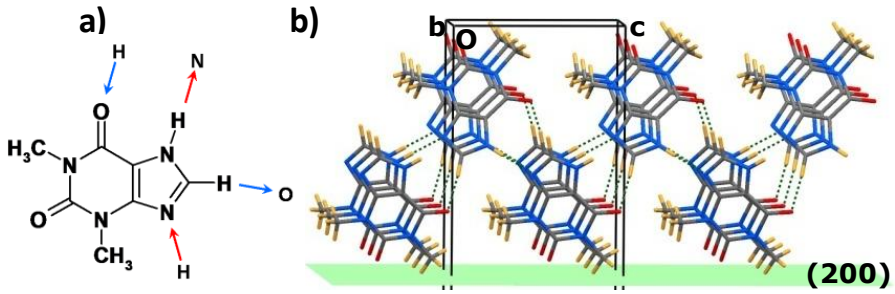

Figure 7. The crystal structure of the anhydrous form of theophylline. (a) The hydrogen bonds around a single molecule; the red and blue arrows indicate two distinct hydrogen bonds. (b) A molecular bilayer parallel to the *bc* plane; C gray, H yellow, N blue, O red; the green dotted lines indicate hydrogen bonds. Note the exposed non-hydrogen bonded carbonyl groups at the (200) plane.

We theorized that hydrophilic functional groups present at the solution-SAM interface could interact with the exposed third acceptors present on the {200} faces of growing crystallites (**Figure 7**). These interactions serve to stabilize the growing nuclei by reducing the possibility of dissolution and enhancing the growth rate of this less stable modification. Powder X-ray diffraction (PXRD) analysis corroborates this theory by showing an increase in the intensity of the (200) reflections relative to other reflections when crystals were grown in the presence of SAMs **3**-**5**.

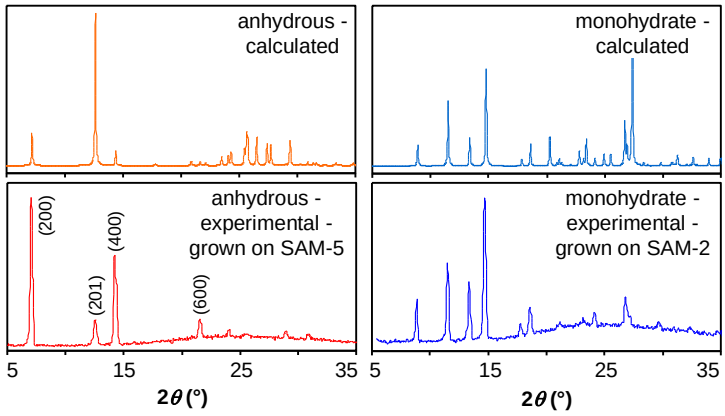

Figure 8. Top: Calculated PXRD diffraction patterns[22] of the anhydrous (left) and monohydrate (right) forms of theophylline. Bottom: experimental PXRD patterns of the two forms on SAMs **5** (left) and **2** (right). Note the differences in the relative intensities of various peaks, particularly those labeled, in the calculated and experimental patterns of the anhydrous form.

Noting the apparent face selectivity between the {200} faces and hydrophilic SAMs **3-5,** we sought to evaluate if the two dimensional periodicity of the substrate was involved in the observed results. To assess the role of the substrate geometry we conducted a set of crystallization trials using glass slides bearing hydroxyl functional groups under similar conditions observed with the SAM trials. In these experiments, we observed concomitant growth of the anhydrous and monohydrate modifications with the anhydrous form being the predominate form obtained. These experiments suggest an epitaxial interaction between the anhydrous form and SAMs **3-5**.

We used EpiCalc,[23] a lattice matching program, to examine the geometric complementarity between hydrophilic monolayers and the crystal faces. All surfaces used in this study possess the same two dimensional periodicity ($a_1 = a_2 = 4.97$ Å and $\alpha = 120°$). The software generates an overlayer lattice (b_1, b_2, β) comprised of the crystal face being examined, and rotates this layer over the substrate lattice through a series of azimuthal angles (EpiCalc theory and calculations are described in section 2.5.4). During overlayer rotation, a dimensionless potential is calculated (V/V_o) that indicates the type and level of epitaxy between the two lattices. Our analysis indicates that the {200}, {201}, {111} and {011} faces of the anhydrous form exhibit ideal coincident epitaxy with the SAM surfaces and that the {200} face has the smallest supercell area demonstrating the best epitaxial relationship of all the faces examined (Table 1).

Table 1. Parameters for geometric epitaxy.

polymorph	face	basic cell[a]			supercell[b]		θ(°)	V/V_o
		b_1(Å)	b_2(Å)	β(°)	multi-pliers[c]	area (Å^2)		
anhydrous	{200}	3.830	8.501	90	4 × 1	130.2	24.20	0.50
	{110}	8.501	24.908	90	1 × 1	211.7	30.25	0.52
	{201}	3.830	29.914	90	2 × 4	916.6	34.18	0.50
	{111}	9.324	24.908	93.62	2 × 4	1854.2	53.10	0.50
	{011}	9.324	24.612	90	4 × 3	2753.8	58.07	0.50
monohydrate	{101}	14.423	15.355	90	1 × 1	221.5	58.20	0.55
	{011}	4.468	20.197	95	1 × 3	269.7	45.75	0.50
	{110}	13.121	15.992	92.17	1 × 2	419.4	20.10	0.52
	{020}	4.468	13.121	97.79	4 × 2	464.7	46.75	0.54
	{10 $\bar{1}$ }	13.275	15.355	90	3 × 3	1834.5	49.15	0.50
	{11 $\bar{1}$ }	20.197	22.794	95.95	3 × 4	5494.7	54.70	0.48

Inspection of the monohydrate faces with EpiCalc yielded only two instances of ideal coincident epitaxy, {011} and {10$\bar{1}$}, other faces deviate from the ideal value of $V/V_o = 0.50$.

As mentioned earlier, the water molecules present in the monohydrate provide the necessary hydrogen bond donors to complement the idle acceptors (**Figure 9**). That is, there are no exposed hydrogen bond donors or acceptors present in the monohydrate that are easily accessible making the likelihood of nucleating the monohydrate on SAMs **3-5** remote.

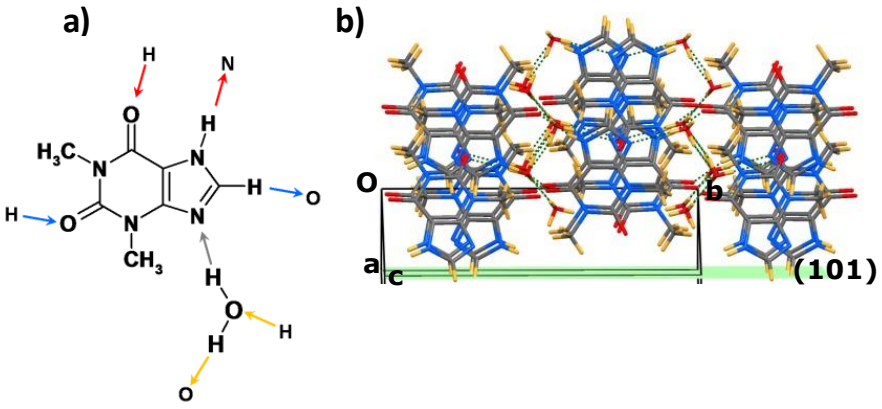

Figure 9. The crystal structure of the monohydrate form of theophylline. (a) The hydrogen bonds around a single molecule; the red, yellow and blue arrows indicate three distinct hydrogen bonds. Note that all potential donors and acceptors participate in hydrogen bonding. (b) The corrugated packing of the molecules; C gray, H yellow, N blue, O red; the green dotted lines indicate hydrogen bonds. Note the absence of exposed acceptors at the (101) interface. One of the hydrogen atoms of the water molecule is disordered.

Interestingly, when crystallization took place in the presence of hydrophobic SAMs **1** and **2** the monohydrate was obtained almost exclusively, suggesting a possible epitaxial match between growth faces and the surfaces. Investigation of the lattice registry using EpiCalc suggested a possible epitaxial match between the {101} faces and SAMs **1** and **2**. Noting this possibility, we investigated the orientation of theophylline molecules in the (101) plane of the monohydrate (**Figure 9**). The molecules pack in a corrugated fashion exposing =CH and CH_3 groups, these groups may interact favorably with SAMs **1** and **2** due to the mutual hydrophobicity of the surfaces and the functionalities exposed at the crystal faces. Powder X-ray diffraction analyses did not yield any instances of face selective growth of the monohydrate on any of the surfaces.

2.3 Preparation of SAMs

Gold coated glass slides purchased from Evaporated Metal Films had two layers of metal coating: a 50 Å thick chromium adhesive layer and a 1000 Å thick gold layer. The slides had a thickness of 1 mm; they were cut into 25 mm × 37.5 mm pieces and immersed in a freshly prepared piranha solution (70% conc. H_2SO_4 and 30% aqueous H_2O_2) at 90°C. After 10 minutes the slides were taken out, rinsed with deionized water and ethanol, and dried with a stream of nitrogen *(caution: piranha solution reacts violently with organic compounds and should not be stored in closed containers; it should be used only in fume hoods)*. The SAMs **1**-**5** (**Figure 4**) were fabricated by immersing these cleaned gold slides in 1 mM ethanolic solutions of the ω-functionalized thiols. After 8-16 h the substrates were taken from the solution and rinsed with copious amounts of ethanol and blown dry with a stream of nitrogen. Freshly prepared SAM substrates were used in the characterization and crystal growth experiments.

2.4 Characterization of SAMs

A thorough characterization of the surfaces was performed to check the extent of coverage, hydrophobicity and hydrophilicity of surfaces, the relative thickness of SAMs, and the identity of the monolayer components.

2.4.1 Contact Angles were measured at nine different positions for each type of surface (three separate slides) with a manual goniometer (Rame-Hart, Model 100-00). The values reported in Table 1 were averages of these measurements. Deionized water droplets (5 μL) were added to each surface using a calibrated Epindorf pipette and the angles obtained had a maximum error of ± 1.6°. The contact angles provided a rough measure of hydrophobicity and hydrophilicity of the surfaces.

Table 2. Contact angle and ellipsometric data for SAMs **1**-**5**.

SAM	Thiol	Contact Angle	Thickness (Å)
1	dodecanethiol	96.2 ± 1.6°	14.2 ± 1.2
2	hexadecanethiol	98.4 ± 0.6°	22.0 ± 1.0
3	11-mercaptoundecanol	33.5 ± 1.2°	14.6 ± 1.1
4	11-mercaptoundecanoic acid	29.6 ± 0.8°	18.3 ± 1.3
5	16-mercaptohexadecanoic acid	28.4 ± 0.6°	21.8 ± 1.2
-	bare gold	76.0 ± 0.9°	-

2.4.2 Ellipsometry measurements were performed on a manual photoelectric ellipsometer (Rudoph Instruments, Model 439L633P). Thickness data reported in Table 2 were estimated assuming a refractive index of 1.462 and an extinction coefficient of 0 for all the substrates. The data were taken as averages of nine different spots on three separate slides for each type of surface. The measurements used a He-Ne laser (λ = 6328 Å) that fell at a 70° angle on the substrate and reflected into the analyzer.

2.4.3 Infrared Spectra of SAMs were collected with a Nexus FT-IR spectrometer (Model 670) equipped with a liquid nitrogen cooled MCTA detector and a ThermoNicolet grazing incidence accessory. Nitrogen gas was used to purge the optical path before and during data acquisition. For each sample 64 scans with a 4 cm^{-1} resolution were collected using an IR laser incident at an angle of 75°. Increasing the number of scans up to 480 did not significantly change the intensity of peaks. **Figure 10** shows IR spectra of SAMs in the fingerprint region. A freshly prepared gold substrate was used as background prior to the acquisition of each IR spectrum. These spectra clearly show the identity of the SAMs formed on gold substrates. The bending/wagging vibrations of methylene groups were seen in all the spectra. In SAM-**3**, C–O stretching was seen at 1180 cm^{-1}; in SAMs **4** and **5** C=O stretching appeared at 1710 and 1712 cm^{-1} respectively.

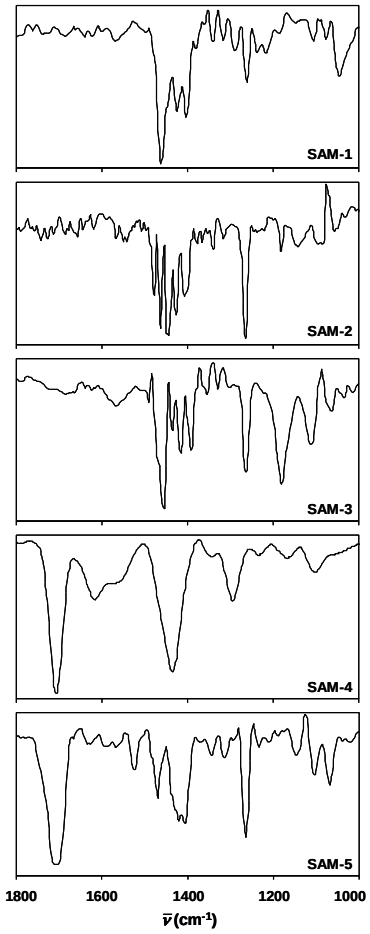

Figure 10. Grazing angle IR spectra of SAMs **1**-**5**. The plots used wave numbers on the *x*-axes and % reflectance on the *y* axes.

2.4.4 Cyclic Voltammetry experiments were carried out using a potentiostat/galvanostat (EG&G Princeton Applied Research Model 273). A three-electrode setup, wherein the SAM/gold substrate clamped with an alligator clip acted as the working electrode, and SCE and Pt wire acted as reference and counter electrodes, was used in these measurements. A 1 mM solution of $K_3[Fe(CN)_6]$ was used as the redox active material with 50 mM KCl as the supporting electrolyte. Both solutions were freshly prepared and bubbled with nitrogen gas for 15 min. The complete electrochemical cell was placed in a Faraday cage to minimize noise. The CV curves were obtained in the range -0.5 to +0.7 V with a scan rate 50 mVs^{-1} and a 1 mV scan increment (**Figure 11**). When bare gold was used as a substrate the CV measurement showed the redox activity Fe^{3+}/Fe^{2+} couple; for SAM coated gold substrates the measurements showed near zero activity indicating that the gold slides were fully covered with the SAMs.

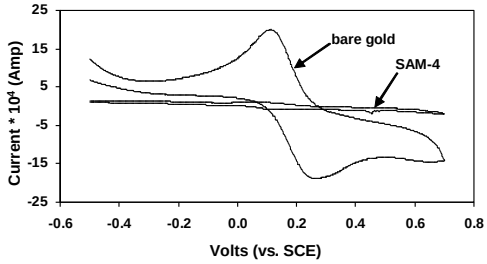

Figure 11. Redox activity of Fe^{3+}/Fe^{2+} couple in cyclic voltammetry when bare gold and SAM substrates acted as working electrodes.

2.5 Crystal Growth on SAMs

In a 100 mL beaker, nearly saturated theophylline solution was made in ethanol (200 proof, Pharmco) and heated at 60 °C for 30 minutes. The solution was cooled to 20 °C and transferred to 20 mL glass vials containing SAMs. Gold coated slides exposing SAMs were leaned at 50-90° angles against the walls of the vials. The solution was added until the slides were completely immersed and the vials were covered with a punctured aluminum foil to allow slow evaporation. All the crystal growth experiments were performed in parallel and at least five times at 20 °C and ~70% relative humidity. The results in all these experiments were qualitatively similar. Crystals of monohydrate and anhydrous form appeared about the same time, typically between 24-36 h.

One concern with crystallization by evaporation is that a metastable polymorph (in this case the anhydrous form) formed in the beginning may not be able to transform to a stable form (in this case the monohydrate) if all the solvent is evaporated. Use of alternative crystal growth methods (such as cooling or anti-solvent addition) may promote any possible phase transitions. We performed the crystal growth experiments (by slow evaporation of the solvent) on hydrophobic and hydrophilic SAMs in parallel using the same crystallization solution. These experiments are carried out multiple times to check for consistency. If the crystal growth method (and not the SAMs) is responsible for the selective growth, we should have observed such selectivity irrespective of the type of SAM substrate used. The reproducibility of our results (hydrogen bonding SAMs – anhydrous form; hydrophobic SAMs – monohydrate) shows that it is the nature of the SAMs (and not the growth method) that is responsible for the observed selectivity.

Once the crystals appeared on SAMs, the substrates were slowly withdrawn from the vial and gently blown with nitrogen gas to detach any physisorbed crystals and particles. The crystals that were still attached to the substrate were carefully dislodged and immediately used in the characterization experiments. We observed that crystals were more tightly adhered to SAMs **3**-**5** than SAMs **1**-**2**. This observation again indicates a higher degree of interfacial interactions in the case of hydrophilic SAMs. Crystals of monohydrate grew on hydrophobic SAMs **1**-**2** as well as on the surfaces of the vial containing these SAMs. In the case of hydrophilic SAMs **3**-**5**, crystals of anhydrous form appeared on the SAM

surfaces whereas crystals of anhydrous and monohydrate form were grown on the vial surfaces. In the absence of SAMs (with or without bare gold substrates immersed in solution) concomitant crystallization of both forms took place; monohydrate was the predominant form. We used bare gold substrates as controls in all the experiments. Typically, very few crystals were formed on these substrates. More than 95% of these crystals belong to the monohydrate form. This is in accordance with the hydrophobicity of bare gold substrates.

We also performed the crystal growth experiments of theophylline in 0.01-10 μm solutions of thiols 1-5. The objective of this exercise was to determine if thiol molecules dissolved in solution had the same effect as the SAMs **1-5** on a surface. Powder X-ray diffraction analysis showed that these experiments resulted in a concomitant mixture of anhydrous (~15-20%) and monohydrate (80-85%) forms. Similar results were obtained in the absence of thiol molecules dissolved in solution.

2.5.1 Infrared Spectra of Polymorphs were collected with a Perkin Elmer FT-IR spectrometer (Model: Spectrum One) fitted with an ATR accessory. We used IR as the first characterization tool because the ATR accessory allowed rapid data acquisition (< 1 min) with a small amount of sample (< 5 mg). The two polymorphs under consideration can be clearly identified from the spectra (**Figure 12**); the most distinguishable peak corresponds to the broad O–H stretching frequency of water in the monohydrate at 3450 cm^{-1}.

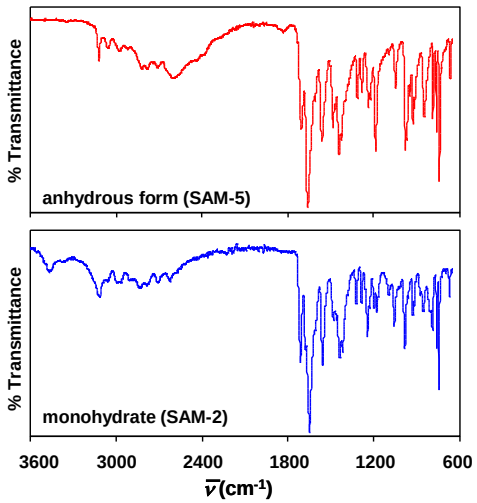

Figure 12. IR spectra of monohydrate and anhydrous forms of theophylline grown on SAMs.

2.5.2 Differential Scanning Calorimetry measurements were carried out with DSC-2920 (TA Instruments) in hermetically sealed and crimped aluminum pans. Samples were subjected to heating in the range 30-300 °C at a rate of 10 °C per minute (**Figure 13**). The monohydrate showed a distinct endotherm near 70 °C corresponding to

the loss of water; the anhydrous form showed no such endotherm. Both forms displayed no further phase transitions until the melting endotherm, which appeared at 272 °C. Thermal gravimetric analysis (TGA-2950, TA Instruments) of the monohydrate showed that the endotherm at 70 °C in DSC corresponds to complete loss of water.

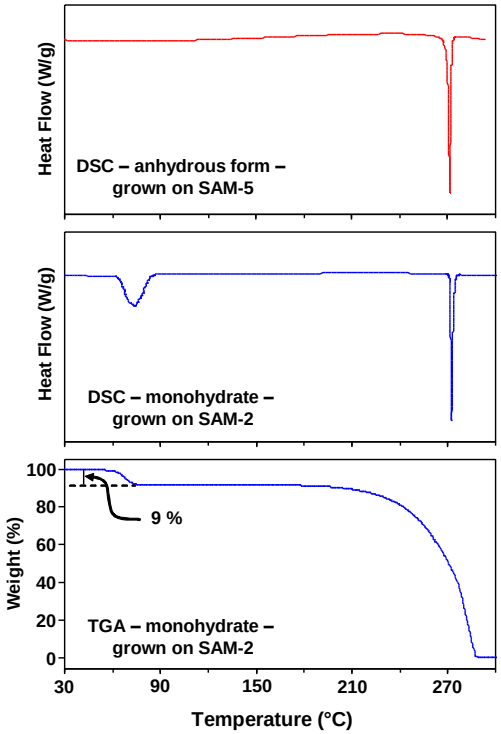

Figure 13. Thermal analysis of monohydrate and anhydrous forms of theophylline. Notice the complete dehydration at 70 °C in the monohydrate.

2.5.3 Powder X-Ray Diffraction data were collected on a Rigaku Geigerflex D-MAX/A diffractometer using Cu-Kα radiation. The instrument was equipped with a vertical goniometer and a scintillation counter as a detector and applied Bragg-Brentano geometry for data collection. X-rays were generated at a power setting of 35 kV and 35 mA. Crystals of the anhydrous form grown on SAMs were usually small (50-100 μm); these were used for diffraction directly. If the crystals were larger (as in the case of monohydrate) they were pulverized using a mortar and a pestle prior to diffraction analysis. We also subjected the smaller crystals of monohydrate to diffraction without grinding; there was no significant change in the relative intensities of the diffraction peaks. Samples were transferred to a glass sample holder that had loading dimensions 1.6 cm × 2 cm and exposed to X-rays over the 2θ range 5-50° in 0.05° steps and at a scan rate of 2° per minute.

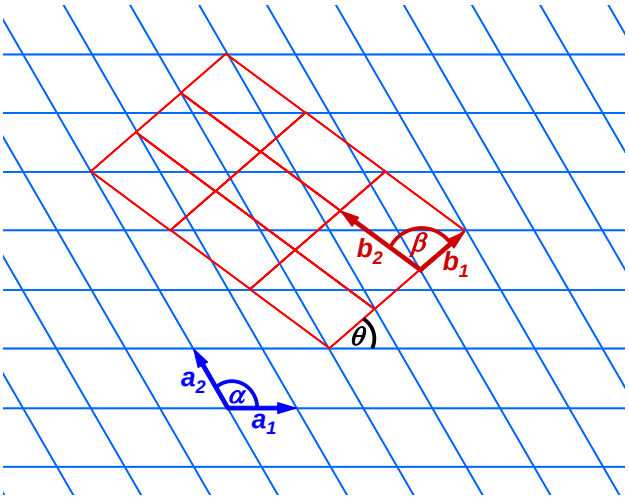

Figure 14. Schematic representation of coincident epitaxy. Substrate lattice (a_1, a_2, α) is drawn in blue; overlayer lattice (b_1, b_2, β) is drawn in red. Note that the vertices of a 3 × 3 supercell of the overlayer lattice reside on corners of the substrate lattice.

2.5.4 Geometric Epitaxy was determined by the lattice matching program EpiCalc. Complete description of the program and its various applications can be found in the elegant original papers published by Ward and coworkers.[23] A brief overview is provided here to guide the reader to understand the results presented in Table 1. EpiCalc determines the lattice registry by rotating an overlayer lattice (b_1, b_2, β) on a substrate lattice (a_1, a_2, α) through a series of azimuthal angles (θ) (**Figure 14**). For each azimuthal angle, the program calculates a dimensionless potential V/V_o, whose value depends on the type of epitaxy between the two lattices (Table 3).

Table 3. Dependence of value of V/V_o on the type of epitaxy.

V/V_o	Epitaxy	Symmetry of Substrate Lattice
1	incommensurate	any
0.5	coincident	any
0	commensurate	non-hexagonal
-0.5	commensurate	hexagonal

Commensurate epitaxy, an ideal form of epitaxy, involves the matching of every lattice point of the overlayer with the substrate lattice points. Coincident epitaxy, less ideal but more common form of epitaxy, involves the matching of some lattice points of the overlayer with substrate lattice points. One way to look at coincident epitaxy is that a supercell (an integral multiple of basic unit cell; e.g., 3 x 3 supercell in **Figure 14**) of overlayer exhibits commensurate epitaxy with the substrate. It follows then that the smaller the size of the supercell greater is the epitaxial match between two lattices. If the two lattices do not exhibit commensurate or coincident epitaxy, they are said to be incommensurate.

2.6 Summary

We showed that hydrogen bonding SAMs act as templates for the selective growth of the thermodynamically less stable anhydrous form of theophylline. We believe that several properties inherent to the anhydrous form, (i) an imbalance in the number of hydrogen bond donors and acceptors, (ii) layered arrangement of molecules exposing the excess acceptors at the largest growing face, and (iii) serendipitous coincident epitaxy, led to this selectivity.

Selective growth of polymorphs from solution is still an empirical process that requires lengthy and time consuming efforts. We hope this approach, and approaches by other groups, will help to elucidate the factors that contribute to epitaxy and selective crystal growth using designer templates. We also note that this approach, and others like it, are challenged by nucleation at sites other than the desired template. These adventitious templates, whether they are dust particles or scratches in the surface of the crystallization vessel, need to be minimized in order to increase the selectivity of a designer template.

3 SUPPRESSED NUCLEATION - INDOMETHACIN

3.1 Background

There have been reports in the literature of polymorphs that were once grown with ease and then suddenly, without significant alterations in procedure, could no longer be obtained. These 'disappearing polymorphs' as they are called, are replaced by new forms that are thermodynamically more stable and once nucleated, grow at the expense of the 'disappearing forms'.[24] This process, known as Ostwald ripening,[25] was responsible for the late stage phase transformation of Norvir® (described in **Section 1.4**) that resulted in deleterious consequences for Abbott Laboratories. Issues like the one with Norvir, have prompted the FDA to require rigorous polymorph screening for all new drugs to prevent this situation from happening again. However, without the proper screening approaches, one may never isolate the most stable polymorph of a given drug.

A common strategy to avoid late stage phase transformations is to screen for new polymorphs, especially the more stable modifications, early in the formulation stage of drug discovery. In our earlier work (**Section 2**), we noted the impact of adventitious templates in the nucleation of different polymorphs. Bearing this point in mind, we fabricated surfaces bearing perfluoroalkyl functional groups (PF) that are not known to form favorable contacts with any other functional groups except other fluorinated functionalities. We chose to use silane monolayers on hydroxylated surfaces because this type of surfactant/substrate system would allow us to fabricate monolayers inside the entire crystallization vessel.

Indomethacin, a non steroidal anti-inflammatory drug (NSAID), crystallizes concomitantly from ethanol in two modifications – α and γ.[26] The stable of the two modifications, the γ form, was obtained exclusively on surfaces bearing the PF functionality. We demonstrate that the observed results are due to the suppressed nucleation of the metastable α form. We also show that fabricating these surfaces on the entire crystallization surface (monolayer covers entire interior of vial, test tube, etc.) results in improved polymorphic selectivity.

3.2 Results

Two methods, using nine different surfaces, were employed to investigate the effects of templates on the crystal growth of indomethacin. In **method 1**, we deposited the monolayer on to plasma-oxidized glass slides. The glass slides were tilted at 0°and 50° angles with respect to the bottom of the vial inside vials containing nearly saturated ethanolic solutions of indomethacin. **Method 2** consisted of fabricating monolayers inside walls of the crystallization vessels, followed by crystal growth under the same conditions outlined in **method 1**. The two methods are depicted schematically in **Figure 15**. Silane monolayers differ from thiol SAMs in a number of respects, the most striking difference is that silane surfaces lack long range order. That is, the surface does not exhibit any two dimensional periodicity that may lead to geometric epitaxy.

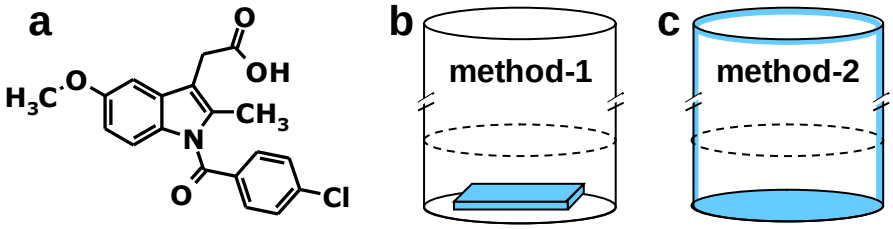

Figure 15. (a) Molecular structure of indomethacin. (b,c) Schematic depictions of the two methods used in this work. Light blue shading corresponds to monolayer coverage; dashed lines denote air solution interface.

Silane monolayers are ideal candidates for this work because each surfactant molecule forms covalent bonds with the substrate that can be deposited onto any hydroxyl-bearing surface – particularly glass substrates.[27] In addition to the functionalities listed in **Figure 16**, we also used bare glass (**1**) and plasma-oxidized glass (**2**) as control surfaces.

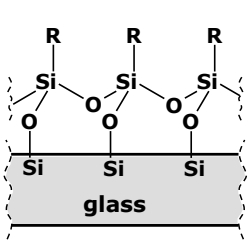

3: R = $-CH_2CH_2CO_2CH_3$
4: R = $-CH_2CH_2CH_2C{\equiv}N$
5: R = $-CH_2CH_2CH_2Cl$
6: R = $-C_6H_4CH_2Cl$
7: R = $-(CH_2)_9CH{=}CH_2$
8: R = $-(CH_2)_{17}CH_3$
9: R = $-(CH_2)_2(CF)_4CF_3$

Figure 16. Representation of siloxane network on a glass substrate (left). Network formed after the reaction of various trichlorosilanes used in this work (right) with hydroxylated glass substrates in the presence of trace amounts of moisture.

Using **method 1** we observed that surfaces **1**-**8** yielded mixtures of both forms on the substrates with considerable polycrystalline growth along the vial walls. Surface **9** however, yielded a singular morphology on the surface of the monolayers with the same polycrystalline growth present on the vial walls observed previously during trials with surfaces **1**-**8**. PXRD and ATR-IR spectroscopy studies revealed that the singular morphology (plates) formed on substrate **9** was the γ polymorph. The polycrystalline film present on the vial walls was primarily the α modification. Optical micrographs summarizing these results are displayed in **Figure 17**.

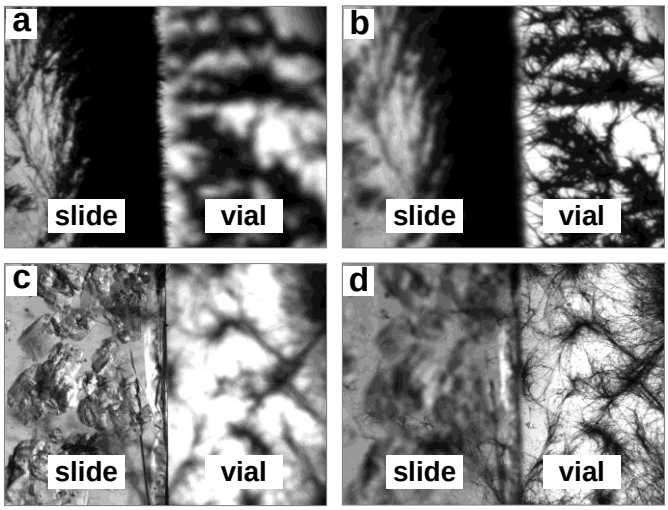

Figure 17. Indomethacin crystal growth by using **method 1**. Slides functionalized with silane monolayers are on the left side of the images. The right portions of the images show the bottoms of the vials not covered by the slides. (a,b) Crystal growth on **5** monolayers with focus on the slide (in a) and on the vial (in b). Notice the predominate growth of α polymorph on both locations. (c,d) Crystal growth on **9** monolayers with focus on the slide (c) and on the vial (d). Notice the predominate growth of γ polymorph on the slide and α polymorph at the bottom of the vial.

As can be seen from **Figures 17** and **18**, the two modifications can be distinguished visually based on the morphology present (α-needles; γ-plates). By separating the γ crystals from the total solid material we were able to determine the relative quantity of each polymorph present on the slides and surfaces.

While this procedure lacks 100% accuracy, it avoids the possibility of inducing a phase transformation during grinding. Co-grinding is necessary during phase quantification by PXRD, ATR-IR spectroscopy and differential scanning calorimetry (DSC). Over the course of eight trials, we were able to generate a plot (**Figure 19**) examining the relative quantity of γ present for a given surface.

The analysis of the total solid material illustrates the predominance of γ on substrate **9** (**Figure 19**; ▲ and ■). If we limit our analysis to the quantity of γ present on the slide only (■) the selectivity is clearly more pronounced. Noting the apparent selectivity of **9**, and the predominance of α modification on the vial surfaces, we examined the selectivity of surfaces **1**-**9** using **method 2**.

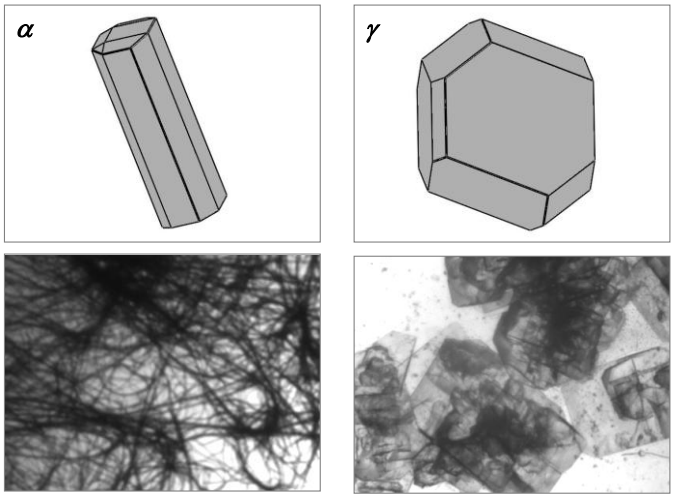

Figure 18. Calculated (top; using BFDH theory) and observed (bottom) morphologies of the α (left) and γ (right) polymorphs of indomethacin.

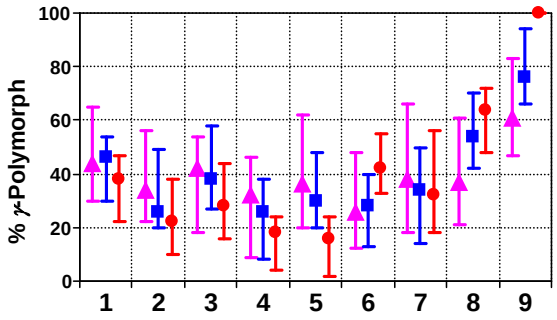

Figure 19. Relative amount of γ polymorph grown on substrates **1**-**9** by using **method 1** (▲: slides plus vials; ■: slides only) and **method 2** (●). The position of the marker indicates the mean over eight experiments; error bars illustrate the largest and smallest quantities of the γ form obtained. Note the exclusive growth (no error bars) of the γ polymorph on substrate **9**.

By functionalizing the entire surface of the crystallization vessel (vial) we hoped to minimize the effects of competing templates. Surfaces **1**-**8** produced concomitant mixtures of both polymorphs in varying proportions depending on the surface in question (**Figure 19**; ●). Perfluorinated surface **9**, however, yielded phase pure γ indomethacin. These results emphasize two points, (i) monolayer **9** selectively nucleates the more stable form of indomethacin and (ii) by eliminating adventitious templates we increased the selectivity.

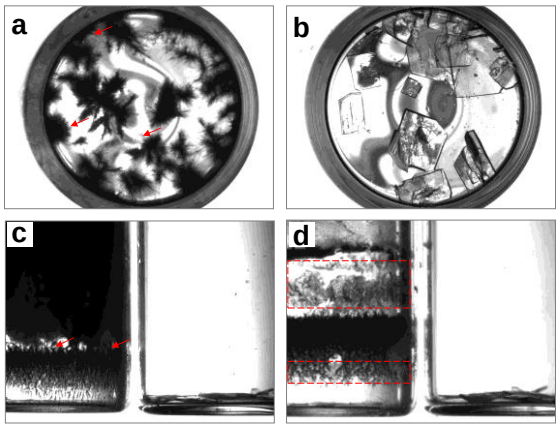

Figure 20. Indomethacin crystal growth using **method 2**. (a-b) View perpendicular to the bottom of the vial showing the crystal growth on **5** (in a) and **9** (in b) monolayers. In this zoomed out view only α crystals are seen in **a**. At a closer view, this vial contains ~10 % of γ crystals. Notice the exclusive growth (and larger size) of γ crystals in **b**. (c-d) View parallel to the bottom of the vial showing the crystals grown on **5** (left vial) and **9** (right vial) monolayers in ethanol (c) and acetonitrile (d) solutions. Notice the rampant crystal growth of the α form on the walls of **5** vials. In contrast, crystal growth is completely inhibited on the walls of **9** vials. Notice the plate-like γ crystals at the bottom of **9** vials. Arrows and boxed areas indicate areas that contain concomitant crystallization.

Noting the marked increase in selectivity using **method 2**, we surmised that by eliminating competing nucleation sites, and choosing a surface that lacks hydrogen bond acceptors and donors (non-stick surface **9**) we increase the likelihood of nucleating the stable modification. Ostwald's rule of stages suggests that less stable forms will nucleate first; however, if stable modifications nucleate, they will grow at the expense of the metastable nuclei, explaining the selectivity in **Figure 19**.

We altered crystallization conditions such as solvent, evaporation rate and temperature, to examine the ability of **method 2** (with substrate **9)** to nucleate the γ polymorph. **Figure 20** (d) illustrates the similarity of the results obtained using either ethanol or acetonitrile as a solvent. Crystallization at slower evaporation rates and lower temperatures (0° C) resulted in qualitatively similar outcomes, albeit an induction time of four days (slow evaporation) and 10 days (0° C), to those reported in **Figure 20**. It is also important to note that the α modification grew on the sides of vials **1**-**8** under both sets of conditions. These results confirm two important findings, (i) α nuclei that form in vials **1**-**8** do not convert to the stable form because they are stabilized by sites on vials **1**-**8** and (ii) α nuclei that form in vial **9** are not stabilized and facilitate the formation and growth of the stable form.

We performed crystal growth experiments in larger vials with smaller S/V ratios (**Figure 25**). Seven of the eight crystallization experiments in 3 dram vials (S/V = 2.83 cm^{-1}) functionalized with **9** monolayers gave only the *γ*-polymorph. In one experiment, *α*-

polymorph (6%) crystallized along with the γ-form. When 20 mL vials (S/V = 2.37 cm^{-1}) functionalized with **9** monolayers were used, crystals of α-polymorph appeared (4-13%) in six of the eight experiments. Two crystal growth experiments done in 100 mL beakers (S/V = 1.21 cm^{-1}) functionalized with **9** monolayers yielded α-polymorph (18% and 24%) along with the γ-polymorph in both the experiments. Thus, the current method is effective when vials with high S/V ratios are used for crystal growth. Our work shows that researchers aiming to crystallize stable polymorphs will have higher chances of success at their attempts if they use narrow tubular vessels (with high values of S/V ratios) functionalized with **9** or other related perfluoroalkyl monolayers.

3.3 Preparation of Substrates

3.3.1 Materials (2-Carbomethoxy)ethyltrichlorosilane (**3**) was purchased from Oakwood Products Inc. and used as received. (3-Cyanopropyl)trichlorosilane (**4**) and (1*H*,1*H*,2*H*,2*H*-perfluorooctyl)trichlorosilane (**9**) were purchased from Aldrich and used without further purification. (3-Chloropropyl)trichlorosilane (**5**), (4-chloromethyl)phenyltrichlorosilane (**6**), and indomethacin were purchased from Alfa Aesar and used without further purification. 10-Undecenyltrichlorosilane (**7**) was purchased from Gelest Inc. and used as received. *n*-Octadecyltrichlorosilane (**8**) was purchased from TCI America and used as received. Absolute ethanol and HPLC grade toluene were purchased from Pharmco and used as received. Precleaned 25 × 75 × 1 mm and 50 × 75 × 1 mm glass microscope slides were purchased from VWR and ½ dram (1.85 mL), 3 dram (11.09 mL) and 20 mL precleaned glass vials were purchased from Kimble and Wheaton Scientific and used as received. The vials were sold in these different denominations (dram and mL); in the following sections we refer to the vials using the naming given above.

3.3.2 Preparation of Substrates and Plasma Oxidation Glass microscope slide substrates were prepared by cutting the slides into 1 × 10 × 15 mm strips. These strips and glass vials (to be used as silane substrates) were oxidized for approximately two minutes under an oxygen plasma using a plasma etcher (SPI Plasma Prep II) that was operating at 13.56 MHz under a 200 micron vacuum. Plasma oxidation of glass substrates is a well established process; it creates surfaces exposing silanol groups (**Figure 21**). After the completion of plasma oxidation, the mild vacuum inside the plasma chamber was maintained (to avoid contamination from outside moisture) until the glass slides and vials were ready for monolayer deposition. All the substrates (slides and vials) were oxidized immediately prior to monolayer deposition.

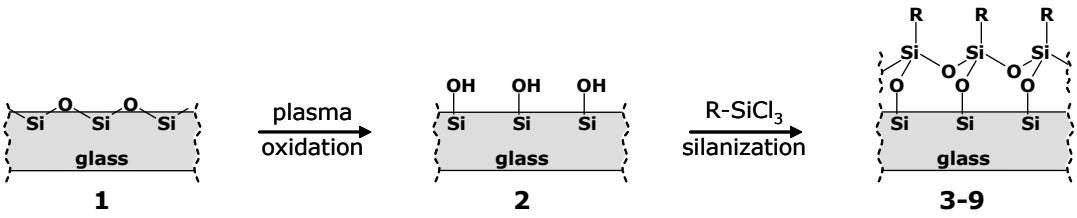

Figure 21. Schematic representation of plasma oxidation of glass substrates and silanization with trichlorosilane derivatives.

3.3.3 Fabrication of Silane Monolayers on Glass Slide Substrates

Trichlorosilane **(**R-$SiCl_3$) solutions (~1 mM) were freshly prepared in toluene and transferred to 20 mL glass vials. Freshly oxidized glass slide strips were removed from the plasma etcher and immersed in the trichlorosilane solutions. The glass vials were completely filled with the silane solutions; they were capped and stored in a cabinet for approximately three hours. The slides were removed from the trichlorosilane solutions, rinsed thoroughly with toluene, and sonicated for 20 minutes in acetone using a Branson 2510 sonicator. After the sonication, the slides were washed with absolute ethanol at least three times and dried under a stream of nitrogen. These slides exposing the silane monolayers at the surface (**Figure 21**) were used for crystal growth within 30 minutes of the fabrication of the monolayers.

3.3.4. Fabrication of Silane Monolayers on the Inner Surfaces of Glass Vials

Freshly prepared ~1 mM toluene solutions of trichlorosilanes were transferred to oxidized ½ dram glass vials that had just been removed from the plasma chamber. The vials were filled completely with silane solutions, capped, and stored in a cabinet. After three hours, the trichlorosilane solutions were pipetted out of the vials using glass Pasteur pipettes. The vials were rinsed thoroughly with toluene, sonicated for 20 minutes in acetone using a Branson 2510 sonicator, washed at least three times with absolute ethanol and dried under a stream of nitrogen. These vials now contained silane monolayers on their inner surfaces (**Figure 21**); they were used for crystal growth experiments within 30 minutes of the fabrication of the monolayers.

3.4 Characterization of Substrates

3.4.1. Contact Angle Measurements

Contact angles were measured at nine different positions for each type of surface (three separate slides) with a manual goniometer (Rame-Hart, Model 100-00). The values reported in Table 3 were averages of these measurements. Deionized water droplets (3 μL) were added to each surface using a calibrated Epindorf pipette and the angles obtained had a maximum error of ± 2.3°. The contact angles show that the surface is modified; they provide a rough measure of hydrophobicity and hydrophilicity of the surfaces.

Table 3. Contact angle data for substrates **1**-**9**.

Substrate	Silane	Contact Angle
1	bare glass	19.3 ± 2.3°
2	plasma treated glass	13.5 ± 2.1°
3	(2-carbomethoxy)ethyltrichlorosilane	42.1 ± 1.8°
4	(3-cyanopropyl)trichlorosilane	56.3 ± 2.2°
5	(3-chloropropyl)trichlorosilane	68.4 ± 1.8°
6	(4-chloromethyl)phenyltrichlorosilane	75.8 ± 1.4°
7	10-undecenyltrichlorosilane	86.7 ± 1.8°
8	*n*-octadecyltrichlorosilane	91.3 ± 1.2°
9	(1*H*,1*H*,2*H*,2*H*-perfluorooctyl)trichlorosilane	104.4 ± 1.1°

3.5 Crystal Growth

3.5.1. Crystal Growth on Glass Slides Bearing Silane Monolayers In a 100 mL beaker, 25 mM indomethacin solution was made in ethanol and heated at 60 °C for 30 minutes. Ethanol was added in excess at the beginning; the volume of the solution was reduced to required concentration by the evaporation of solvent during heating. The solution was cooled to 20 °C and filtered to 20 mL glass vials containing glass slides bearing silane monolayers. The slides were placed at the bottom of the vial as shown in **Figure 15** (b). Each vial was filled with 5 mL of the solution and covered with a perforated aluminum foil to allow the evaporation of the solvent. All the crystal growth experiments were performed at 20 °C in parallel for at least eight times. Crystals of α-polymorph appeared on the vial walls within 10-20 hours in all the cases.

3.5.2. Crystal Growth in Glass Vials Functionalized with Silane Monolayers on the Inner Surfaces Indomethacin solutions (25 mM) were prepared as above and filtered to ½ dram glass vials functionalized with silane monolayers. Each vial was filled with 1.2 mL of the solution and covered with a perforated aluminum foil to allow the slow evaporation of the solvent. All the crystal growth experiments were performed at 20 °C in parallel for at least eight times. The results in all these experiments were qualitatively similar; see **Figure 19** and below for the quantification of the results. Crystals of α-polymorph appeared on the walls of vials **1**-**8** within 14-20 hours in all the cases. In **9** vials, crystals of γ-polymorph appeared at the bottom of the vials in 30-56 hours. In these vials crystal growth did not occur on the vial walls. Commercial indomethacin contained predominantly (> 97 %) γ-polymorph. We also carried out crystallizations in **9** vials using indomethacin solutions that were

prepared from > 99% α-polymorph. In three out of three experiments under these conditions, we observed the exclusive crystal growth of γ-polymorph in **9** vials.

3.5.3. Crystal Growth in Functionalized Glass Vials from Acetonitrile Solutions The procedure is as above except that acetonitrile is used as a solvent instead of ethanol. The concentrations of the solutions were 25 mM. As in the case of ethanol solutions, control vials **1**-**2** and vials functionalized with monolayers **3**-**8** yielded a mixture of α- and γ-polymorphs, whereas the vials functionalized with **9** monolayers produced only the γ-polymorph. We carried out these experiments two times.

3.5.4. Crystal Growth by Slower Evaporation in Functionalized Glass Vials We did two repeats of these experiments using 25 mM ethanol solutions in functionalized ½ dram vials. We sealed the vials with parafilm and made a pinhole in the parafilm with the tip of a needle. The objective here was to retard the rate of evaporation of ethanol and contrast these results with the experiments above. As above, crystals of α-polymorph grew on the walls of vials **1**-**8** and no crystal growth occurred on the walls of **9** vials. The difference in this case is that α-crystals appeared on the walls of vials **1**-**8** after at least *four days*. In **9** vials, γ-crystals appeared at the bottom after five to six days.

3.6 Polymorph Characterization

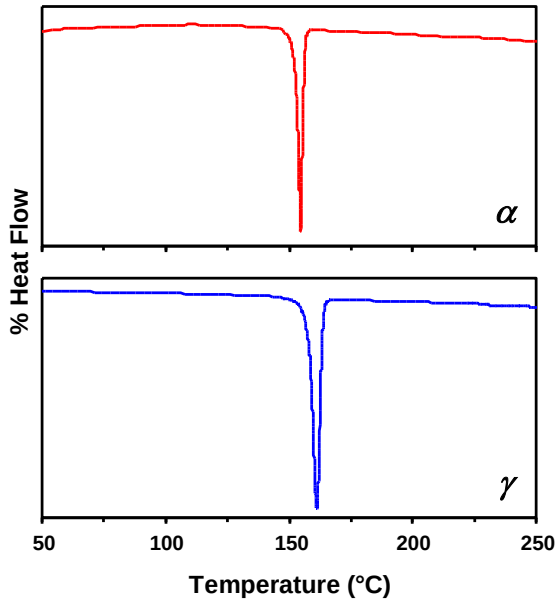

Figure 22. DSC Plots of α- (red, above) and γ-polymorphs (blue, below) showing the melting endotherms. Note that the γ-polymorph melts (158° C) at a slightly higher temperature than the α-form (153° C).

3.6.1. Differential Scanning Calorimetry These measurements were carried out with DSC-2920 (TA Instruments) in hermetically sealed and crimped aluminum pans. Samples were subjected to heating in the range 30-250 °C at a rate of 10 °C per minute (**Figure 22**). The two polymorphs showed distinct endotherms corresponding to their melting; α at 153 °C and γ at 158 °C. These melting points are 2-3° less than the reported values in the literature. No other phase transitions were observed in the temperature range used.

3.6.2. Infrared Spectra of Polymorphs Infrared spectra were collected with a Nexus FT-IR spectrometer (Model 670) equipped with a liquid nitrogen cooled MCTA detector and an ATR accessory. We used IR as the first characterization tool because the ATR accessory allowed rapid data acquisition (< 1 min) with a small amount of sample (< 5 mg). The two polymorphs under consideration can be clearly identified from the IR spectra (**Figure 23**). The α-polymorph crystallizes in a noncentrosymmetric space group ($P2_1$) with three molecules in the asymmetric unit, whereas the γ-polymorph belongs to a centrosymmetric space group ($P\bar{1}$) with one molecule in the asymmetric unit. Consequently the α-polymorph has greater number IR absorptions than the γ-polymorph. A comparison of the two spectra reveals that there are several peaks that distinguish the two polymorphs; the arrows in **Figure 23** indicate the characteristic absorptions used by other researchers to identify the α-polymorph.

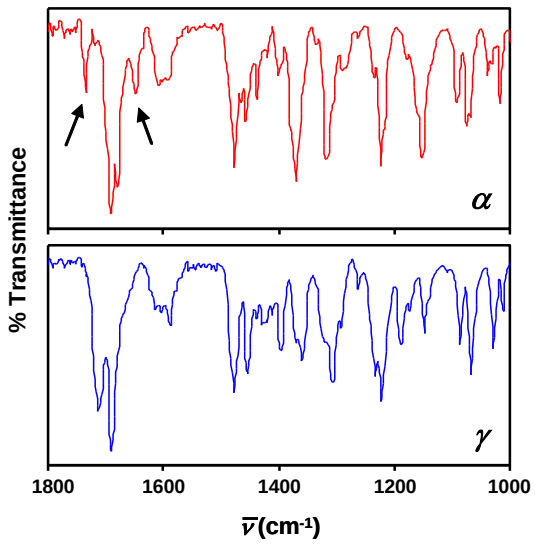

Figure 23. ATR-FT IR Spectra of α- (red, above) and γ-polymorphs (blue, below). Notice the significant differences between the two IR spectra; arrows in the top spectrum show characteristic peaks of α-polymorph.

3.6.3. Powder X-Ray Diffraction Analysis Powder X-ray data were collected on a Rigaku Geigerflex D-MAX/A diffractometer using Cu-$K\alpha$ radiation. The instrument was equipped with a vertical goniometer and a scintillation counter as a detector and

applied Bragg-Brentano geometry for data collection. X-rays were generated at a power setting of 35 kV and 35 mA. Crystals of the α-polymorph were fluffy and small quantities of this polymorph occupied large volumes; the diffraction peaks of this polymorph were usually weaker than the γ-polymorph. The crystals obtained from the experiments above were pulverized using a mortar and a pestle prior to diffraction analysis. Finely ground powders were transferred to a glass sample holder that had loading dimensions 1.6 cm × 2 cm and exposed to X-rays over the 2θ range 5-40° in 0.05° steps and at a scan rate of 2° per minute. **Figure 24** shows the experimental powder patterns along with powder patterns calculated from the single crystal X-ray structures. These X-ray patterns show that the crystals obtained from **9** vials correspond to the γ-polymorph.

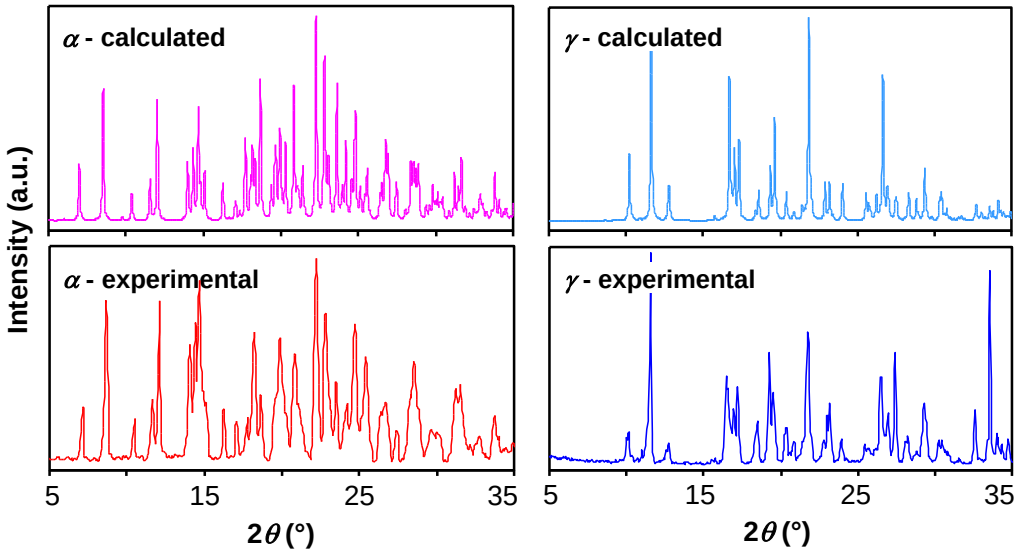

Figure 24. Calculated (top) and experimental (bottom) powder X-ray diffraction patterns of α- (left) and γ-polymorphs (right). The experimental diffraction pattern for the γ-polymorph is taken from the crystals grown in a **9** vial. The experimental diffraction pattern for the α-polymorph is taken from fibrous material collected from a **5** vial. These patterns match well with the diffraction patterns calculated from the single crystal structures.

3.6.4. Quantitative Analysis of α- and γ-polymorphs The crystals of α- and γ-polymorphs have distinct morphologies (see **Figure 18**); we could readily distinguish between the two forms by visual inspection. We separated the crystals of γ-polymorph grown on glass slides and vials with the aid of a pair of tweezers, a surgical blade and microscope. We scraped the solid material from the vial on to a glass slide (50 × 75 mm), spread the crystals, and moved the γ-crystals to a different slide. These separated samples were then weighed on an analytical balance and the weights so obtained were used to calculate the relative amounts of the two polymorphs (**Figure 19**). Separation of this kind invariably left a small portion of α-form in the pile of γ-form and vice versa. This method

is thus approximate and cannot be used for accurate quantitative analysis. The main result of the current study (exclusive growth of the crystals of γ-polymorph on **9** monolayers), however, is unaffected by the inaccuracies of this method. As noted in the **Results**, co-grinding of samples is a prerequisite for the quantification by PXRD and IR spectroscopy; such co-grinding can lead to phase transition between the polymorphs or transition to the amorphous form.

3.6.5. Effect of Surface Area-to-Volume (S/V) Ratio of the Vial on the Crystal Growth

We performed all the experiments described (crystallizations in functionalized vials) using ½ dram vials. Owing to their small sizes, these vials have a high S/V ratio (5.61 cm^{-1}); crystallization in these vials is governed predominantly by heterogeneous nucleation on the surfaces (as opposed to the bulk nucleation in solution).

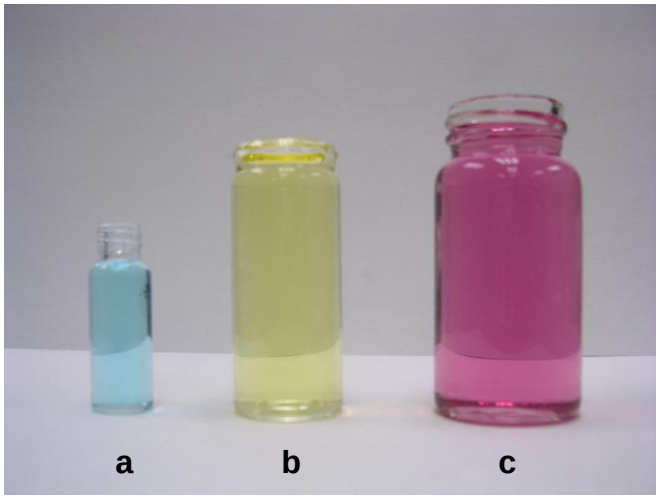

Figure 25. Glass vials (**a**: ½ dram; **b**: 3 dram; **c**: 20 mL) used for indomethacin crystal growth. The vials are filled with aqueous solutions of food dyes to accentuate the contrast between them. Most crystallizations in this work are performed in ½ dram vials.

3.7 Summary

The approach described in this work aims to selectively nucleate the most stable modifications of polymorphic compounds. Our approach is two-fold; (i) use 'non-stick' surfaces to prevent stabilization of metastable nuclei and (ii) fabricate surfaces over entire crystallization vessel, preferably with a high surface area to volume ratio, to eliminate adventitious templates and competing nucleation sites. Indeed, we were able to consistently obtain the more stable γ form of indomethacin utilizing this approach.

This method is facile and does not require pre-requisite knowledge of specific interfacial interactions necessary for template design using other approaches. We believe this approach will aid in polymorph screening of APIs and help to eliminate situations similar to the one encountered by Abbott Laboratories.

We will extend this work to other APIs as well as inorganic compounds to test its generality and wider applicability. Preliminary results suggest that this method is also applicable to organic compounds with heteroatom-containing functional groups.

4 MICROWAVE ASSISTED POLYMORPH SELECTION

4.1 Background

Microwaves are routinely used to assist in chemical processes such as organic synthesis, hydrothermal and solvothermal syntheses, and formation of monodisperse crystallites.[28] The major advantages of microwave heating are increases in reaction rates, improved yields, energy savings, and reduced use of volatile solvents. These advantages are due to 'thermal effects' associated with microwave heating mechanisms. The two integral characteristics of microwave heating that give rise to 'thermal effects' are (i) localized super-heating and (ii) volumetric heating. Localized super-heating refers to regions in a matrix that become much hotter than the bulk of the matrix when exposed to microwave irradiation. Volumetric heating describes the 'inside-out' nature of microwave heating, where the entire matrix heats up rapidly. Convectional heating must heat from the outside inwards.[29]

Little research has focused on the impact of microwave heating on the crystallization of polymorphic organic compounds. Recent work in our group has yielded instances of selective polymorph growth during microwave assisted crystallization. Our work will examine the underlying causes of the observed polymorphic selectivity and will test the applicability of this method to a number of organic compounds with primary focus on APIs.

4.2 Initial Results

We used a domestic microwave oven to heat saturated ethanol solutions of acetaminophen and drive these solutions to supersaturation (solutions were microwaved until the resulting solutions were viscous, duration of irradiation depended on initial saturation level and volume). Following an induction period of approximately 8-15 minutes we observed rapid growth of the metastable form of acetaminophen. This experiment was repeated ten times with same results.

We also repeated these experiments using a hot plate to verify if characteristics solely associated with microwave heating were responsible for the results. In these experiments we placed vials containing ethanolic solutions of acetaminophen onto a digitally controlled hot plate operating at 70° C and evaporated the solvent until the solutions were viscous. The vials were removed and a range of induction times followed (1-9 minutes) that yielded inconsistent results. Of the ten trials, only two runs produced phase pure metastable acetaminophen. The remaining eight trials produced either the stable modification or mixtures of the two forms. These preliminary results are promising but further investigations into the origin of the selectivity are required.

4.3 API Crystallization

We believe that localized super-heating caused by microwave irradiation helps to destroy any pre-existing nuclei in solution. Nuclei are small aggregates or clusters of molecules in solution that may develop and grow into crystals. By destroying all nuclei it is feasible

that we could add small crystals of a particular polymorph, a process known as seeding, and template the growth of that particular form.

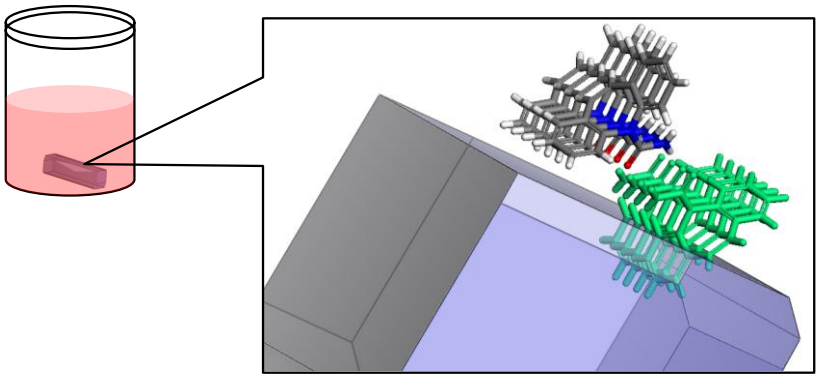

Figure 26. A schematic diagram of seeding and the mechanism by which it operates. (left) A seed has been added to a saturated solution. Note that the seed crystal is quite large in this diagram, this is not representative of the actual size of a seed crystal. Seed crystals are typically much smaller than this – approximately 40 μm in each dimension. (right) The magnified view depicts a face of the seed crystal acting as a template to promote the growth of that particular face. Green molecules represent molecules that are part of the seed crystal lattice.

Typically, seeding processes compete with the growth of existing nuclei or nuclei that form in solution. We surmise that microwaving saturated solutions of APIs causes two events to take place simultaneously, (i) dissolution of all nuclei and (ii) attainment of high levels of supersaturation. Evolution of a system that is highly supersaturated and lacks the presence of any nuclei is an ideal system to seed. We hope that this method enhances the success of seeding operations with respect to polymorph selectivity and yield.

4.4 Selective Heating and Micro-Emulsions

Microwaves exhibit the unique characteristic of selective heating.[29] That is, one or more components in a mixture may be microwave susceptible (or heat up during irradiation) while the remaining components are microwave transparent (unaffected by microwave irradiation). We would like to create micro-emulsions comprised of microwave susceptible droplets inside a microwave transparent matrix. The droplets would be solutions of an API and will be driven to supersaturation as the solvent heats up and evaporates. A potential example would be dissolving acetaminophen in ethanol and creating an emulsion with mineral oil. The emulsion could then be irradiated with microwaves thereby heating the ethanolic droplets and increasing the saturation level of acetaminophen until crystallization occurs. We theorize that by encapsulating the API solution in a chosen media and selectively heating that component, we can eliminate adventitious templates and alter the crystallization environment by working with different

microwave transparent media. By controlling the size and size distribution of the droplets we may also be able to control the resulting morphology and narrow the size distribution of crystallites.

5 REFERENCES

(1) Mitscherlich, E., *Annales de Chimie*, **1822**, 19, 350–419.

(2) W. C. McCrone, *Polymorphism in Physics and Chemistry of the Organic Solid State, Vol. 2*, ed. D. Fox and M. M. Labes, Weinberger, Interscience, New York, **1965**, p. 725

(3) G. R. Desiraju, *CrystEngComm* **2003,** *5*, 466-467; K. R. Seddon, *Cryst. Growth Des.* **2004,** *4*, 1087; G. R. Desiraju, *Cryst. Growth Des.* **2004,** *4*, 1089-1090; J. Bernstein, *Cryst. Growth Des.* **2005,** *5*, 1661-1662; A. Nangia, *Cryst. Growth Des.* **2006,** *6*, 2-4.

(4) Crystal structures were obtained from the Cambridge Structural Database. The Refcode for form I: **HXACAN06**. Refcode for form II: **HXACAN08**.

(5) S. R. Byrn; R. R. Pfeiffer; J. G. Stowell, *Solid-State Chemistry of Drugs*. 2nd ed.; SSCI: West Lafayette, **1999**.

(6) H. G. Brittain, Ed. *Polymorphism in Pharmaceutical Solids*. Marcel Dekker: New York, **1999**; R. Hilfiker, Ed. *Polymorphism in the Pharmaceutical Industry*. Wiley-VCH: Weinheim, **2006**.

(7) Chemburkar, S. R., et al., *Org. Process Res. Dev.* **2000,** *4*, 413-417; Miller, J. M.; Collman, B. M.; Greene, L. R.; Grant, D. J. W.; Blackburn, A. C., *Pharm. Dev. Technol.* **2005,** *10*, 291-297.

(8) J. Bernstein, *'Polymorphism in Molecular Crystals'*, Clarendon Press, Oxford, **2002**, Chapter 10.

(9) S. L. Morissette; S. Soukasene; D. Levinson; M. J. Cima; O. Almarsson, *Proc. Nat. Acad. Sci.* **2003,** *100*, 2180-2184.

(10) I.V. Markov, *Crystal Growth for Beginners: Fundamentals of Nucleation, Crystal Growth and Epitaxy*, World Scientific, Singapore, New Jersey, London, Hong Kong **1995**.

(11) M. Lahav; L. Addadi; L. Leiserowitz, *Proc. Nat. Acad. Sci.* **1987,** *84*, 4737-4738.

(12) L. M. Frostman; M. M. Bader; M. D. Ward, *Langmuir* **1994,** *10*, 576-582; F. C. Meldrum; J. Flath; W. Knoll, *Langmuir* **1997,** *13*, 2033-2049; J. Kuther; R. Seshadri; W. Knoll; W. Tremel, *J. Mater. Chem.* **1998,** *8*, 641-650; J. Aizenberg; A. J. Black; G. M. Whitesides, *J. Am. Chem. Soc.* **1999,** *121*, 4500-4509; A. Y. Lee; A. Ulman; A. S. Myerson, *Langmuir* **2002,** *18*, 5886-5898; N. Banno; T. Nakanishi; M. Matsunaga; T. Asahi; T. Osaka, *J. Am. Chem. Soc.* **2004,** *126*, 428-429; R. Hiremath; S. W. Varney; J. A. Swift, *Chem. Comm.* **2004**, 2676-2677; R. Hiremath; J. A. Basile; S. W. Varney; J. A. Swift, *J. Am. Chem. Soc.* **2005,** *127*, 18321-18327.

(13) A. C. Hillier; M. D. Ward, *Phys. Rev. B* **1996,** *54*, 14037-14051.

(14) R. G. Nuzzo, B. R. Zegarski, L. H. Dubois. *J. Am. Chem. Soc.*; **1987**; 109(3); 733-740.

(15) C. P. Price; A. L. Grzesiak; A. J. Matzger, *J. Am. Chem. Soc.* **2005,** *127*, 5512-5517.

(16) J. Zaccaro, J. Matic, A.S. Myerson, B.A. Garetz. *Crystal Growth & Design,* **1** (1), 5 - 8, 2001

(17) F.P.A. Fabbiani, D.R. Allan, S. Parsons, C.R. Pulham, *CrystEngComm*, **2004**, 6, 504., F.P.A. Fabbiani, D.R. Allan, S. Parsons, C.R. Pulham, *CrystEngComm*., **2005**, 7, 179.

(18) L. J. Chyall, J. M. Tower, D. A. Coates, T. L. Houston, S. L. Childs, *Cryst. Growth Des.* **2002**, 2, 505-510., J. L. Hilden, C. E. Reyes, M. J. Kelm, J. S. Tan, J. G.

Stowell, K. R. Morris, *Cryst. Growth Des.* **2003**, 3, 921-926., J.-M. Ha, J. H. Wolf, M. A. Hillmyer, M. D Ward,. *J. Am. Chem. Soc.* **2004**, 126, 3382-3383.
(19) J.W. Jenne, *Chest*, **1987**, 92, 7S-14S.
(20) D. J. Sutor, *Acta Cryst.* **1956,** *9*, 969-70; A. A. Naqvi; G. C. Bhattacharyya, *J. Appl. Cryst.* **1981,** *14*, 464.
(21) J. Bernstein; R. J. Davey; J.-O. Henck, *Angew. Chem. Int. Ed.* **1999,** *38*, 3441-3461., N. V. Phadnis; R. Suryanarayanan, *J. Pharm. Sci.* **1997,** *86*, 1256-1263.
(22) Crystal structures were obtained from the Cambridge Structural Database. The Refcode for anhydrous form: **BAPLOT01**. Refcode for monohydrate: **THEOPH01**.
(23) J. A. Last; D. E. Hooks; A. C. Hillier; M. D. Ward, *J. Phys. Chem. B* **1999,** *103*, 6723-6733.
(24) Dunitz, J. D.; Bernstein, J., *Acc. Chem. Res.* **1995,** *28*, 193-200.
(25) Ostwald, W., *Z. Phys. Chem.* **1897,** *22*, 289-330; Threlfall, T., *Org. Process Res. Dev.* **2003,** *7*, 1017-1027.
(26) Legendre, B.; Feutelais, Y., *J. Therm. Anal. Chem.* **2004,** *76*, 255-264.
(27) Carter, P. W.; Ward, M. D., *J. Am. Chem. Soc.* **1994,** *116*, 769-770.
(28) F. Mavandadi, A. Pilotti, *Drug Discovery Today*, **2006**, 11(3 & 4), 165-174., D. Adam, *Nature* (London, United Kingdom), **2003,** 421(6923), 571-572.
(29) W.C. Conner, G.A. Tompsett, *Journal of Physical Chemistry B*, **2008**, 112(7), 2110-2118.